


Article

Timescales Associated with the Evolution of Reactive Scalar Gradient in Premixed Turbulent Combustion: A Direct Numerical Simulation Analysis

Nilanjan Chakraborty ^{1,*}  and Cesar Dopazo ²¹ School of Engineering, Newcastle University, Claremont Road, Newcastle upon Tyne NE1 7RU, UK² School of Engineering and Architecture-Fluid Mechanics Area, University of Zaragoza, 50001 Zaragoza, Spain; cesar.dopazo.garcia@gmail.com

* Correspondence: nilanjan.chakraborty@ncl.ac.uk; Tel.: +44-191-208-3570

Abstract: The fractional change in the reaction progress variable gradient depends on the flow normal straining within the flame and also upon the corresponding normal gradients of the reaction rate and its molecular diffusion transport. The statistical behaviours of the normal strain rate and the contributions arising from the normal gradients of the reaction rate and molecular diffusion rate within the flame were analysed by means of a Direct Numerical Simulation (DNS) database of statistically planar turbulent premixed flames ranging from the wrinkled/corrugated flamelets regime to the thin reaction zones regime. The interaction of flame-normal straining with the flame-normal gradient of molecular diffusion rate was found to govern the reactive scalar gradient transport in the preheat zone, where comparable timescales for turbulent straining and molecular diffusion are obtained for small values of Karlovitz numbers. However, the molecular diffusion timescale turns out to be smaller than the turbulent straining timescale for high values of Karlovitz numbers. By contrast, the reaction and hot product zones of the flame remain mostly unaffected by turbulence, and the reactive scalar gradient transport in this zone is determined by the interaction between the flame-normal gradients of molecular diffusion and chemical reaction rates.

Keywords: turbulent premixed combustion; reactive scalar gradient; molecular diffusion rate; flame normal strain rate; reaction progress variable; direct numerical simulation



Citation: Chakraborty, N.; Dopazo, C. Timescales Associated with the Evolution of Reactive Scalar Gradient in Premixed Turbulent Combustion: A Direct Numerical Simulation Analysis. *Fire* **2024**, *7*, 73. <https://doi.org/10.3390/fire7030073>

Academic Editor: Ali Cemal Benim

Received: 19 January 2024

Revised: 21 February 2024

Accepted: 26 February 2024

Published: 29 February 2024



Copyright: © 2024 by the authors. Licensee MDPI, Basel, Switzerland. This article is an open access article distributed under the terms and conditions of the Creative Commons Attribution (CC BY) license (<https://creativecommons.org/licenses/by/4.0/>).

1. Introduction

The evolution of the reactive scalar gradient magnitude is related to the inverse of three characteristic times: a turbulence timescale, a molecular diffusion time and chemical time. This paper examines the relative magnitudes of these timescales associated with local normal straining, molecular diffusion and chemical reaction contributions to the magnitude of the reaction progress variable gradient evolution for different values of the Karlovitz number. Although several previous studies [1–9] focused on the various aspects of the transport of the reactive scalar gradient, the characteristic times associated with different physical processes associated with its evolution are yet to be scrutinized for different regimes of premixed turbulent combustion. This gap in the existing literature is addressed in this paper by considering the intertwining of small-scale turbulent convection, molecular diffusion and chemical reaction to generate/destroy scalar gradients for different Karlovitz numbers using DNS data of freely propagating statistically planar turbulent premixed flames. In this respect, the main objectives of the present analysis are as follows: (1) to quantify the mean behaviour of the terms of the transport equation of the reactive scalar gradient originating from fluid-dynamic straining, molecular diffusion rate and chemical reaction rate; (2) to identify the timescales associated with the different terms of the transport equation of the reactive scalar gradient using DNS data; and (3) to indicate the

leading order contributions at different regions of the flame front for turbulent premixed flames in different combustion regimes.

The physical behaviour and statistical variations of the reactive scalar gradient are of pivotal importance in the fundamental understanding and modelling of premixed turbulent combustion [1]. The reactive scalar gradient is closely related to the Flame Surface Density (FSD) [2] and Scalar Dissipation Rate (SDR) [2], which are widely used for the modelling of turbulent premixed combustion. The SDR characterises the rate of micro-mixing of scalars. Thus, scalar fluctuations and scalar-fluctuation gradients are intimately linked in turbulent mixing. The pocket formation in premixed turbulent combustion was analysed using the transport equation of the magnitude of the reactive scalar gradient by Kollmann and Chen [3]. The statistical behaviours of the terms of the transport equation of the magnitude of the reaction progress variable gradient and their local curvature and tangential strain rate dependences were investigated by Chakraborty and Cant [4] using Direct Numerical Simulation (DNS) data. The results of Chakraborty and Cant [4] were found to be in qualitative agreement with the detailed chemistry DNS analysis by Chakraborty et al. [5]. Sankaran et al. [6] also analysed the transport characteristics of the reactive scalar gradient magnitude using DNS data of turbulent slot jet premixed flames. Dopazo et al. [7] demonstrated the role of flame propagation in the flame normal straining in the reactive scalar transport in premixed turbulent flames. Wang et al. [8] and Sandeep et al. [9] studied the behaviours of strain rates influencing the evolution of the magnitude of the reactive scalar gradient in laboratory-scale configurations for premixed turbulent flames.

The rest of the paper is organised in the following manner. The mathematical background and numerical implementation related to the current analysis are provided in Sections 2 and 3, respectively. The results are presented and discussed in Section 4 and, finally, the main findings are summarised and conclusions are drawn in Section 5.

2. Mathematical Background

The chemical state within a turbulent premixed flame is characterised by a reaction progress variable c , which can be defined based on a suitable major species mass fraction Y_α in the following manner: $c = (Y_\alpha - Y_{\alpha u}) / (Y_{\alpha b} - Y_{\alpha u})$ (here, subscripts 'u' and 'b' refer to the values in unburned and burned gases, respectively). The reaction progress variable c increases monotonically from 0 to 1.0 from the unburned gas to the fully burned products. The transport equation of c is given by [1–9]:

$$\rho \frac{\partial c}{\partial t} + \rho u_k \frac{\partial c}{\partial x_k} = \frac{\partial}{\partial x_k} \left(\rho D \frac{\partial c}{\partial x_k} \right) + \dot{\omega}_c \quad (1)$$

where ρ is the gas density, u_k is the k th component of fluid velocity, D is the diffusivity and $\dot{\omega}_c$ is the reaction rate of reaction progress variable. Equation (1) can be written in kinematic mode for a given c isosurface as [7–9]:

$$d^c c / dt = [\partial c / \partial t + V_j \partial c / \partial x_j] = 0 \quad (2)$$

where $d^c(\dots)/dt$ corresponds to a total derivative in a reference frame, which is attached to the corresponding c isosurface and $V_j = u_j + S_d N_j$ is the j th component of the isosurface propagation velocity, with S_d and $N_j = -(\partial c / \partial x_j) / |\nabla c|$ being the displacement speed and j th component of the normal vector, respectively. Using $V_j = u_j + S_d N_j$ in Equation (2) yields [7–9]:

$$[\partial c / \partial t + u_j \partial c / \partial x_j] = S_d |\nabla c| \quad (3)$$

A comparison between Equations (1) and (3) provides the expression for the flame displacement speed S_d for a given c isosurface, as follows:

$$S_d = [\dot{\omega}_c + \nabla \cdot (\rho D \nabla c)] / \rho |\nabla c| \quad (4)$$

Upon taking the gradient of both sides of Equation (2), it is possible to define a transport equation of $|\nabla c|$ in the following manner [7–9]:

$$d^c |\nabla c| / dt = -(a_N + N_j \partial S_d / \partial x_j) |\nabla c| \tag{5}$$

where $a_N = N_i N_j \partial u_i / \partial x_j = N_i N_j S_{ij}$ is the fluid-dynamic strain rate normal to the isosurface c , with $S_{ij} = 0.5(\partial u_i / \partial x_j + \partial u_j / \partial x_i)$ being the ij th component of the strain rate tensor. Equation (5) can be rewritten as follows:

$$\frac{1}{|\nabla c|} \left(\frac{\partial |\nabla c|}{\partial t} + u_j \frac{\partial |\nabla c|}{\partial x_j} \right) = -a_N + T_1 + T_2 \tag{6}$$

where T_1 and T_2 are given by the following:

$$T_1 = -\frac{1}{|\nabla c|} \frac{\partial}{\partial x_N} \left[\frac{1}{\rho} \frac{\partial}{\partial x_j} \left(\rho D \frac{\partial c}{\partial x_j} \right) \right] = -\frac{1}{|\nabla c|} \frac{\partial}{\partial x_N} \left[\frac{1}{\rho} \frac{\partial}{\partial x_N} \left(\rho D \frac{\partial c}{\partial x_N} \right) + D \frac{\partial c}{\partial x_N} 2\kappa_m \right] \tag{7}$$

$$T_2 = -\frac{1}{|\nabla c|} \frac{\partial}{\partial x_N} \left(\frac{\dot{\omega}_c}{\rho} \right) \tag{8}$$

Here, T_1 and T_2 represent the generation or destruction of $|\nabla c|$ by molecular diffusion and chemical reaction, respectively, x_N is the local coordinate normal to a given c isosurface pointing toward the fresh reactants and $\kappa_m = 0.5(\partial N_i / \partial x_i)$ is the local isosurface curvature. The magnitudes of T_1 and T_2 can be taken to represent the inverse of timescales associated with molecular diffusion and chemical reaction rates (i.e., $\tau_{md} = 1/|T_1|$ and $\tau_{ch} = 1/|T_2|$), respectively. Equation (7) also allows us to distinguish between two molecular diffusion times, associated with normal and tangential (related to curvature) diffusions, respectively.

From Equations (6)–(8), one might conjecture the existence of two possible zones within the flame:

- (1) Reaction–diffusion zone: Wherever $[a_N] \ll [T_2]$ within the flow domain, the chemical reaction would dominate over the fluid-dynamic strain rate to create or destruct $|\nabla c|$. Molecular diffusion and chemical reaction would be of the same order, which leads to

$$\frac{1}{|\nabla c|} \left(\frac{\partial |\nabla c|}{\partial t} + u_j \frac{\partial |\nabla c|}{\partial x_j} \right) = T_1 + T_2 \tag{9}$$

The turbulent time would be much greater than the reaction and the molecular diffusion times in this zone.

- (2) Convective–diffusive zone: Wherever, $[a_N] \gg [T_2]$ within the flow domain, the fluid-dynamic strain rate would dominate over the chemical reaction to create or destruct $|\nabla c|$. Molecular diffusion and fluid-dynamic strain rate would plausibly be of the same order, which leads to

$$\frac{1}{|\nabla c|} \left(\frac{\partial |\nabla c|}{\partial t} + u_j \frac{\partial |\nabla c|}{\partial x_j} \right) = -a_N + T_1 \tag{10}$$

The reaction time would be much greater than the turbulent straining and the molecular diffusion times in this zone. Pure mixing is expected to occur in this zone.

The timescales $\tau_{md} = 1/|T_1|$ and $\tau_{ch} = 1/|T_2|$ are local and instantaneous times, which can be averaged. Given that molecular diffusion and chemical reactions are small-scale processes, it is worthwhile to assess whether a_N should be of the order of the smallest turbulent strain micro-scale. Therefore, it needs to be assessed if a_N is of the order of a Kolmogorov strain rate, that is, the inverse of the Kolmogorov time micro-scale, τ_K . The local and instantaneous τ_K is defined as $\tau_K = (\nu/\varepsilon)^{1/2}$, where the instantaneous kinetic energy dissipation rate is defined as $\varepsilon = 2\nu S_{ij} S_{ij} - (2/3)\nu(S_{kk})^2$ for variable density flows.

Note that for variable density flows, τ_K is closely related to the volumetric dilatation rate, $\nabla \cdot \mathbf{u}$, and it should also be recalled that $2S_{ij}S_{ij} > (2/3)(\nabla \cdot \mathbf{u})^2$. The relative importance of turbulent strain micro-scale and chemical reaction to generate/destroy scalar gradients, measured by the ratio $|a_N|/|T_2|$, can then be expressed as $|a_N|/|T_2| = \tau_{ch}/\tau_{flow}$, where $\tau_{flow} \sim 1/|a_N|$ is the flow timescale. This is a dimensionless variable, similar to a gradient-related local Karlovitz number if $\tau_{flow} \sim \tau_K$ but with a rather different definition of the characteristic chemical reaction time as $\tau_{ch} = 1/|T_2| = 1/|-(1/|\nabla c|)d(\dot{\omega}_c/\rho)/dx_N|$. For both $\tau_{flow} \gg \tau_{ch}$ (within the reaction zone of the flame) and $\tau_{flow} \ll \tau_{ch}$ (within the preheat zone of the flame), the direct interaction between turbulence and reaction would be very weak. The molecular diffusion time, τ_{md} , should plausibly be of the same order as the smaller of τ_{flow} and τ_{ch} . Small-scale turbulence interacts directly with molecular diffusion in the preheat zone, whereas the reaction directly interacts with molecular diffusion in the reaction zone.

The magnitudes of these timescales and the aforementioned assumptions will be explored in Section 4 of this paper using DNS data of statistically planar turbulent premixed flames for a range of different values of conventional global Karlovitz numbers.

3. Numerical Implementation

The statistical behaviours of a_N , T_1 and T_2 are analysed in this paper using DNS data of statistically planar premixed flames. The simulations used for the current analysis are conducted using a 3D compressible code known as SENGAs+ [10], where all the standard governing equations of reacting flow [11] are solved in non-dimensional form. In SENGAs+, all the spatial differentiations are approximated by a 10th-order central difference scheme for the internal grid points, but the order of accuracy drops gradually to a one-sided 2nd-order scheme at the non-periodic boundaries. The time advancement is achieved using an explicit third-order Runge–Kutta scheme [12]. The simulation domain consists of inlet and outlet boundaries in the direction of mean flame propagation (i.e., x -direction), and the transverse boundaries are considered to be periodic. A partially non-reflecting outlet boundary condition is specified in accordance with the Navier–Stokes Characteristic Boundary Conditions (NSCBC) technique [13]. The mean inlet velocity U_{mean} at the inlet boundary is modified during the simulation in order to make it equal to the turbulent burning velocity so that the flame remains stationary inside the simulation domain. The fluctuating velocity field is initialised by a homogeneous isotropic incompressible field generated by a pseudo-spectral method [14] following the Batchelor–Townsend spectrum [15] for desired values of root mean square turbulent velocity u' and the integral length scale of turbulence l . A steady, unstretched laminar flame solution is used to initialize the scalar field. A modified bandwidth forcing [16] in physical space is used to force the turbulence in the unburned gas to maintain the desired values of root mean square velocity u' and the integral length scale of turbulence l in the unburned gas. The domain size, the uniform Cartesian grid for discretization and the unburned gas values of root mean square turbulent velocity fluctuation normalised by the unstrained laminar burning velocity u'/S_L , integral length scale to the Zel'dovich flame thickness ratio l/δ_z , Damköhler number $Da = lS_L/u'\delta_z$, Karlovitz number $Ka = (u'/S_L)^{3/2}(l/\delta_z)^{-1/2}$ and heat release parameter $\sigma = (T_{ad} - T_0)/T_0$ are listed in Table 1. Here, the Zel'dovich flame thickness δ_z is defined as $\delta_z = \alpha_{T0}/S_L$ with α_{T0} and S_L being the thermal diffusivity and unstrained laminar burning velocity, respectively. The regime of the combustion for the cases according to the Borghi–Peters diagram [17] are also mentioned in Table 1, which indicates that the cases considered here span from the wrinkled flamelet regime to the high Karlovitz number thin reaction zones regime. At least 10 grid points are kept within $\delta_{th} = (T_{ad} - T_0)/\max|\nabla T|_L$ (where T , T_0 and T_{ad} are the dimensional temperature, unburned gas temperature and adiabatic flame temperature, respectively) for the grid used in these simulations, whereas 1.0–2.0 grid points are accommodated within the Kolmogorov length scale η for the turbulence parameters considered here.

Table 1. Simulation parameters for all cases considered in this analysis.

Case	u'/S_L	l/δ_z	Da	Ka	σ	Domain Size	Grid Size
Case—A	1.0	5.25	5.25	0.44	4.5	$140.7\delta_z \times (70.35\delta_z)^2$	$800 \times (400)^2$
Case—B	3.0	5.25	1.75	2.27	4.5	$140.7\delta_z \times (70.35\delta_z)^2$	$800 \times (400)^2$
Case—C	5.0	5.25	1.05	4.88	4.5	$140.7\delta_z \times (70.35\delta_z)^2$	$800 \times (400)^2$
Case—D	7.5	5.25	0.7	8.96	4.5	$140.7\delta_z \times (70.35\delta_z)^2$	$800 \times (400)^2$
Case—E	10.0	5.25	0.525	13.80	4.5	$140.7\delta_z \times (70.35\delta_z)^2$	$800 \times (400)^2$

A generic single-step Arrhenius mechanism (i.e., *Reactants* \rightarrow *Products*) representing stoichiometric methane–air flame is considered in this analysis for the sake of computational economy in the interest of a detailed parametric analysis. The same approach was undertaken by several authors [11,18–24] in the past. All the gases are taken to be perfect gases, and the Lewis number of all the species is considered to be unity. The Prandtl number is taken to be 0.7, the Zel’dovich number (i.e., $\beta = T_{ac}(T_{ad} - T_0)/T_{ad}^2$, where T_{ac} is the activation temperature) is 6.0 and the ratio of specific heats for constant pressure and constant volume (i.e., $\gamma = c_p/c_v$) is 1.4 for all the simulations. These non-dimensional parameters appear in the non-dimensional governing equations for compressible reacting flows, and interested readers are referred to Ref. [11] for further discussion in this regard. These values are representative of stoichiometric methane–air combustion for reactants preheated to 415 K. Several previous analyses [4,5,24] demonstrated that the statistics of $|\nabla c|$ obtained from simple chemistry DNS of stoichiometric methane–air premixed flames show good qualitative agreements with the findings from detailed chemistry DNS. Moreover, it was demonstrated by Keil et al. [25] that the turbulent premixed flame propagation is captured qualitatively by the single-step chemistry. The quantitative differences in the flame displacement speed statistics are comparable to the uncertainty that arises due to different choices of reaction progress variables for the detailed chemical mechanism. As the current analysis depends on the statistics of $|\nabla c|$ and displacement speed, it can be expected at least the qualitative behaviours are going to be captured accurately in the presence of simple chemistry.

The simulations for the current analysis were continued until the turbulent burning velocity S_T and flame surface area A_T attained statistically stationary states, and the desired values of both turbulent kinetic energy and integral length scale were obtained in the unburned gas. This simulation time is at least equal to at least 10 eddy turnover times (i.e., $t_{sim} > 10l/ut$), which also is greater than the through-pass time (i.e., $t_{sim} > L_x/U_{mean}$). Each simulation typically needed 80,000 CPU hours. Interested readers are referred to Ref. [26] for further information regarding this database.

4. Results and Discussion

4.1. Flame Morphology

The reaction progress variable c distributions for cases A–E in the $x - y$ midplane are shown in Figure 1a–e, respectively. It can be seen from Figure 1a–e that the flame wrinkling, in general, increases with increasing turbulence intensity u'/S_L . It can be seen from Figure 1a that case A exhibits large-scale wrinkles due to background turbulent fluid motion, but the isosurfaces of c remain parallel to each other, as the internal flame structure remains unaffected by turbulent fluid motion in the wrinkled/corrugated flamelets regime [17], characterised by $\eta > \delta_{th}$. By contrast, the reaction progress variable isosurfaces are not parallel to each other in cases B–E, and local occurrences of flame thickening can be discerned from Figure 1b–e. This behaviour for cases B–E originates as a result of flame thickness being greater than the Kolmogorov length scale η (i.e., $\delta_{th} > \eta$), which allows for local perturbations of the preheat zone by energetic eddies in these cases. As the separation between δ_{th} and η increases with an increasing Karlovitz number Ka , the localised flame thickening and the extent of the perturbation of the flame structure strengthen from case B to case E.

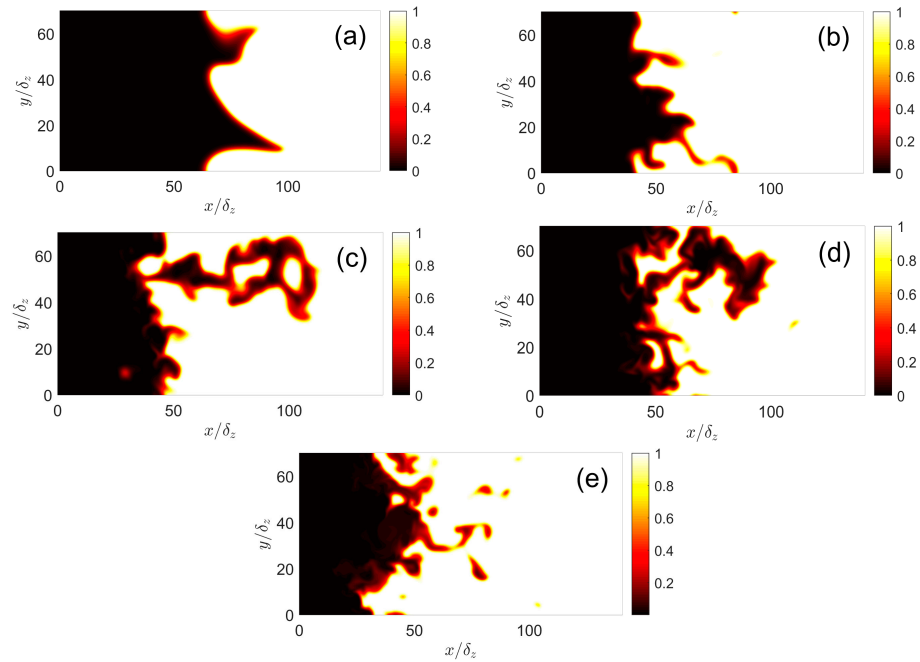


Figure 1. Distribution of c for (a–e) cases A–E in $x - y$ midplane.

4.2. Mean Behaviours of $(-a_N), T_1$ and T_2 Conditioned upon c

Before discussing the behaviours of the timescales associated with T_1 and T_2 , it is worthwhile to present the variations of $\dot{\omega}_c$ and $\nabla \cdot (\rho D \nabla c)$ for the unstretched laminar premixed flame for the thermochemistry of the cases considered here. The variations of $\dot{\omega}_c$, $\nabla \cdot (\rho D \nabla c)$, $\dot{\omega}_c + \nabla \cdot (\rho D \nabla c) = \rho S_d |\nabla c|$ and $\rho_0 S_L |\nabla c|$ with c for the unstretched laminar premixed flame are shown in Figure 2. It can be seen from Figure 2 that $\dot{\omega}_c + \nabla \cdot (\rho D \nabla c) = \rho S_d |\nabla c| \approx \rho_0 S_L |\nabla c|$ is maintained throughout the flame front. Figure 2 shows the chemical reaction rate $\dot{\omega}_c$ assumes significant values for $c > 0.4$, and $\nabla \cdot (\rho D \nabla c)$ takes positive (negative) values for $c < 0.6$ ($c > 0.6$). The reaction rate $\dot{\omega}_c$ and molecular diffusion rate $\nabla \cdot (\rho D \nabla c)$ assume values with similar order of magnitude but with different signs towards the burned gas side, but $\dot{\omega}_c + \nabla \cdot (\rho D \nabla c)$ remains positive throughout the flame front with a peak close to $c = 0.6$. Although the variations in Figure 2 are shown for the steady unstretched laminar premixed flame, the same qualitative (and mostly quantitative) behaviour is observed for the turbulent flame cases considered here, which are not shown here for the sake of conciseness.

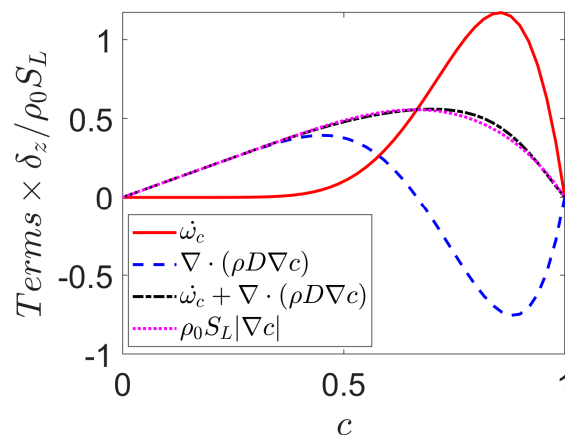


Figure 2. Variations of $\dot{\omega}_c$, $\nabla \cdot (\rho D \nabla c)$, $\dot{\omega}_c + \nabla \cdot (\rho D \nabla c) = \rho S_d |\nabla c|$ and $\rho_0 S_L |\nabla c|$ with c for the unstretched laminar premixed flame for the presented thermochemistry. All the terms are normalised by $\delta_z / \rho_0 S_L$.

The variations of $\dot{\omega}_c$ and $\nabla \cdot (\rho D \nabla c)$ with c determine the behaviour of the mean values of T_1 and T_2 conditional upon c . The variations of the mean values of $\{-a_N, T_1, T_2\} \times \delta_z/S_L$ conditional upon c (i.e., $\{-\langle a_N|c \rangle, \langle T_1|c \rangle, \langle T_2|c \rangle\} \times \delta_z/S_L$) for cases A–E are shown in Figure 3a–e, respectively. The standard deviations of $\{-a_N, T_1, T_2\} \times \delta_z/S_L$, conditional upon c for cases A–E, are also shown with vertical bars in Figure 3a–e. Figure 3a–e show that the mean values of $(-a_N)$, conditional upon c , assumes negative values throughout the flame front. It can be appreciated from $\nabla \cdot (\rho D \nabla c)$ distribution in Figure 2 that $\partial[(1/\rho)\partial(\rho D \partial c/\partial x_j)]/\partial x_N$ is expected to assume a negative (positive) value where $\nabla \cdot (\rho D \nabla c)$ assumes positive (negative) values. Therefore, the mean value of $T_1 = -(1/|\nabla c|)\partial[(1/\rho)\partial(\rho D \partial c/\partial x_j)]/\partial x_N$ conditional upon c assumes a small positive value towards the unburned gas and eventually becomes negative and attains a local minimum around $c = 0.8$ before taking large positive values for $c > 0.9$.

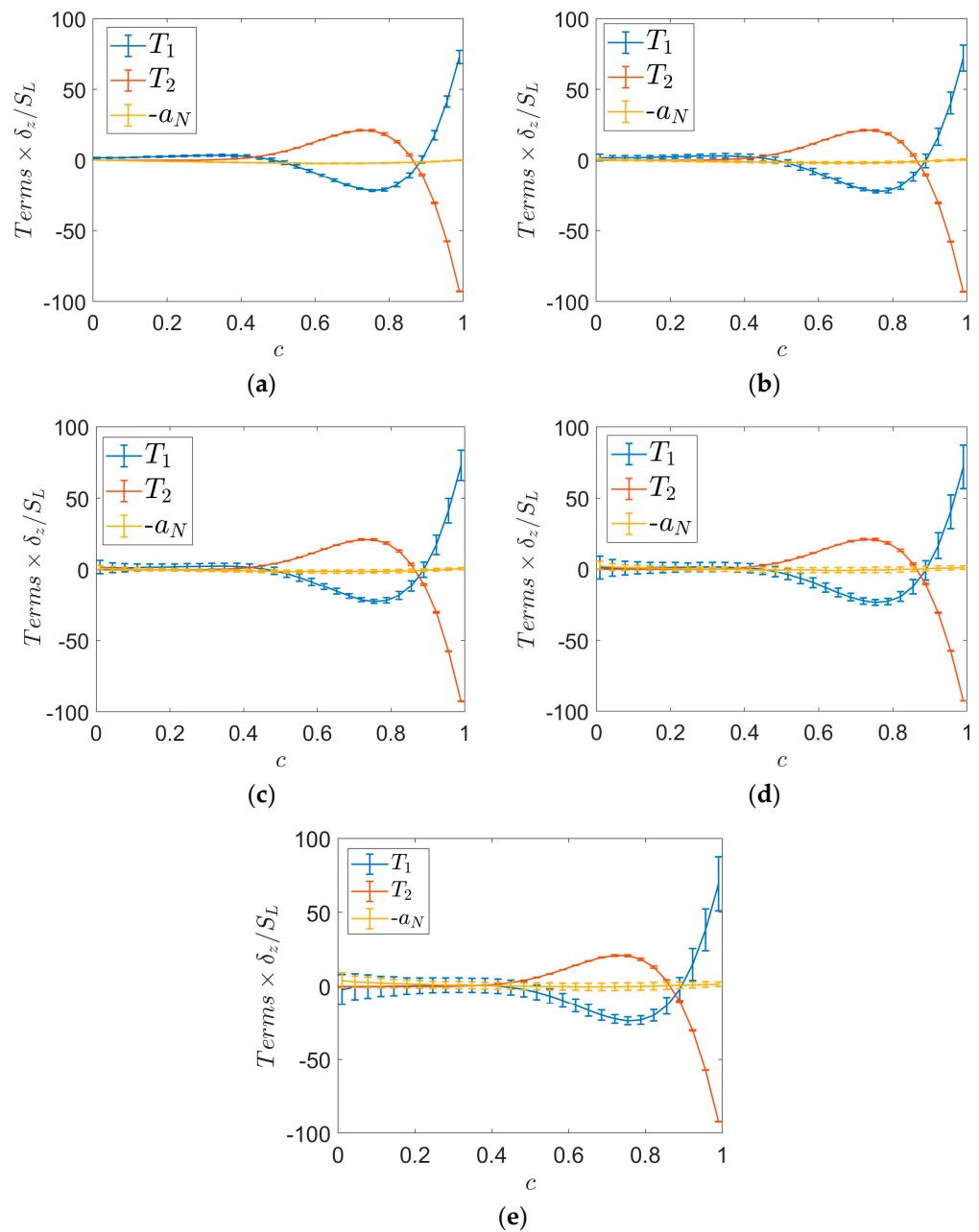


Figure 3. Variations of the normalised mean values of $\{-a_N, T_1, T_2\} \times \delta_z/S_L$ conditional upon c (i.e., $\{-\langle a_N|c \rangle, \langle T_1|c \rangle, \langle T_2|c \rangle\} \times \delta_z/S_L$) for (a–e) cases A–E.

It can be appreciated from Figure 2 that $\partial(\dot{\omega}_c/\rho)/\partial x_N$ is expected to take negative (positive) values before (after) the peak value of $\dot{\omega}_c$ is obtained. Therefore, the mean value of $T_2 = -(1/|\nabla c|)\partial(\dot{\omega}_c/\rho)/\partial x_N$ conditioned upon c assumes small positive value for $c < 0.9$ with a local maximum value around $c = 0.8$ and the mean value of T_2 eventually assuming large negative values for $c > 0.9$ (see Figure 3a–e).

Figure 3a–e reveal that the reaction–diffusion balance (i.e., the balance between T_1 and T_2) is obtained in the reaction zone and the burned gas side (i.e., $c > 0.5$), where $\langle T_1|c \rangle \times \delta_z/S_L$ and $\langle T_2|c \rangle \times \delta_z/S_L$ are of order 10 for $c \geq 0.4 - 0.5$, whereas the contribution of $\langle -a_N|c \rangle$ is much smaller. This is consistent with the expected behaviour of the reaction–diffusion zone (see Equation (9)). On the other hand, for $c < 0.5$, $\langle -a_N|c \rangle$ and of $\langle T_1|c \rangle$ provide non-zero contributions while $\langle T_2|c \rangle$ remains negligible compared to the other two terms.

The terms T_1 and T_2 are associated with small-scale physics, and thus, it is worthwhile to consider whether $\langle T_1|c \rangle$ and $\langle T_2|c \rangle$ scale with the Kolmogorov timescale. The variations of the mean values of $\{-a_N, T_1, T_2\} \times \tau_K$ conditional upon c (i.e., $\{-\langle a_N|c \rangle, \langle T_1|c \rangle, \langle T_2|c \rangle\} \times \tau_K$) for cases A–E are shown in Figure 4a–e, respectively, where τ_K is estimated as $\tau_K = [\langle \nu|c \rangle / \langle \epsilon|c \rangle]^{0.5}$.

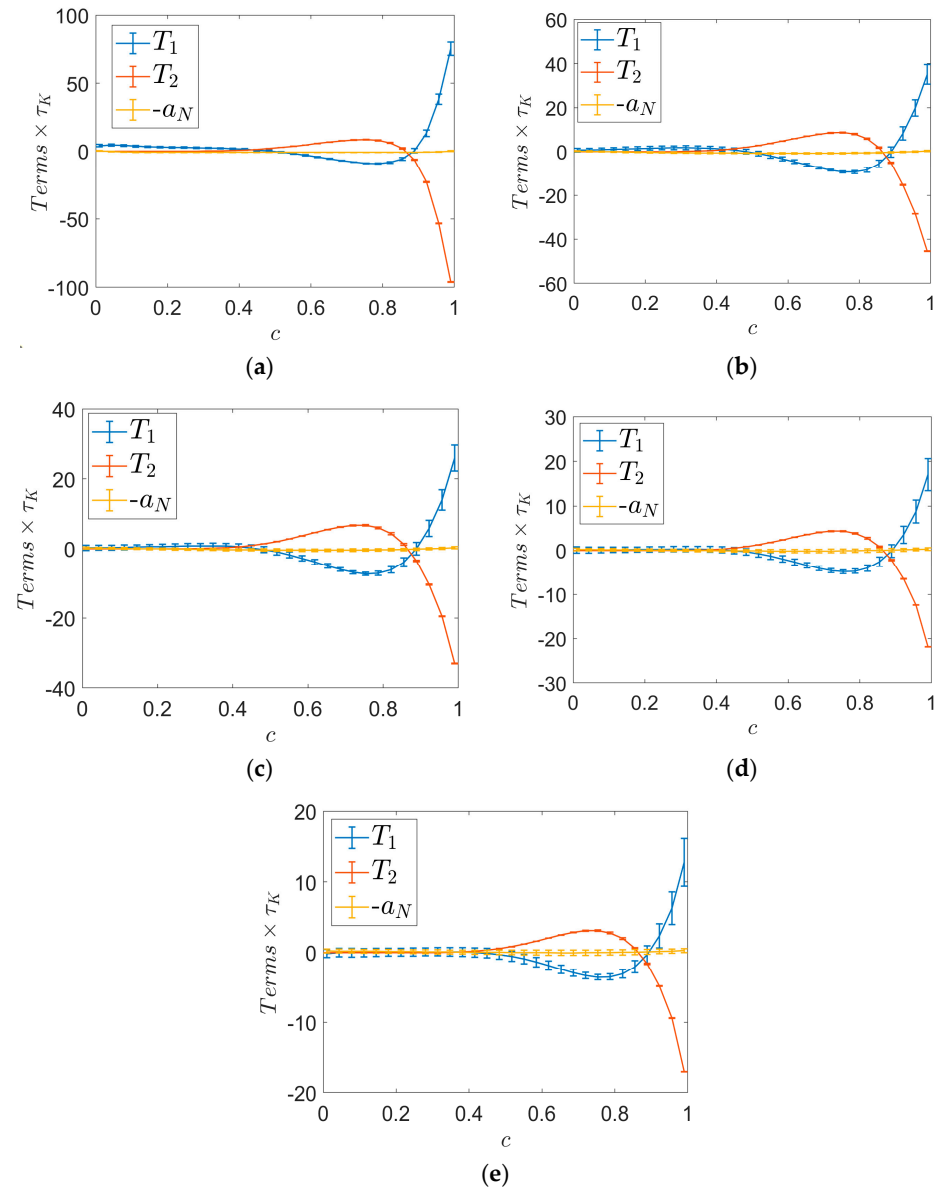


Figure 4. Variations of the normalised mean values of $\{-a_N, T_1, T_2\} \times \tau_K$ conditional upon c (i.e., $\{-\langle a_N|c \rangle, \langle T_1|c \rangle, \langle T_2|c \rangle\} \times \tau_K$) for (a–e) cases A–E.

The qualitative behaviours and leading order balance between $-\langle a_N|c \rangle$, $\langle T_1|c \rangle$ and $\langle T_2|c \rangle$ are not affected by the normalization procedure, as expected. Therefore, the conclusions drawn from Figure 3a–e remain valid also for Figure 4a–e, but the contributions of $\langle T_1|c \rangle \times \tau_K$ and $\langle T_2|c \rangle \times \tau_K$ are approximately of order 1.0 for $c < 0.95$, particularly for high Karlovitz number flames. It can further be seen from Figures 3 and 4 that the standard deviations of $-a_N$, T_1 , T_2 conditioned upon c increases from case A to case E with increasing turbulence intensity.

4.3. Magnitudes of a_N , T_1 and T_2 Conditioned upon c

In order to estimate the timescales associated with $-a_N$, T_1 and T_2 , it is useful to consider the variations of the magnitudes of these quantities across the flame front. The variations of $\langle |a_N||c \rangle \times \delta_z/S_L$ and $\langle |a_N||c \rangle \times \tau_K$ with c are shown in Figures 5 and 6, along with the corresponding standard deviations conditional upon c for cases A–E. It can be seen from both Figures 5 and 6 that $\langle |a_N||c \rangle$ assumes the peak value around $c = 0.7$ for cases A–C, irrespective of the choice of normalization. By contrast, $\langle |a_N||c \rangle \times \delta_z/S_L$ decreases from the unburned gas side of the flame front and fluctuates around of value of unity for the major part of the flame front. In all cases, $\langle |a_N||c \rangle \times \delta_z/S_L$ remains of the order of unity, but the magnitude decreases from case A to case E. In cases D and E, $\langle |a_N||c \rangle \times \tau_K$ fluctuates around 0.29 throughout the flame front, but $\langle |a_N||c \rangle \times \tau_K$ remains of the order of unity for cases A–C.

The normal strain rate a_N can be expressed as [27]

$$a_N = (e_\alpha \cos^2 \theta_\alpha + e_\beta \cos^2 \theta_\beta + e_\gamma \cos^2 \theta_\gamma) \quad (11)$$

where e_α , e_β and e_γ are the most extensive, intermediate and compressive eigenvalues of the strain rate tensor and θ_α , θ_β and θ_γ are the angles between ∇c and the corresponding eigenvectors. It was demonstrated by Chakraborty and Swaminathan [27] that ∇c shows preferential alignment with the eigenvector associated with e_α (i.e., $|\cos \theta_\alpha| = 1.0$) when the strain rate induced by flame normal acceleration ($\sim \sigma S_L/\delta_z$) overwhelms turbulent straining ($\sim u'/l$) [27]. This situation is characterised by $\sigma Da \gg 1$ as the ratio of the strain rate induced by thermal expansion to turbulent straining can be scaled with σDa [27]. By contrast, turbulent straining dominates over the strain rate induced by flame normal acceleration for $\sigma Da \ll 1$, where ∇c preferentially aligns with the eigenvector associated with e_γ (i.e., $|\cos \theta_\gamma| = 1.0$) [27], similar to passive scalar mixing [28–30]. Moreover, Chakraborty and Swaminathan [27] also demonstrated, based on DNS data, that the extent of preferential alignment of ∇c with the eigenvector associated with e_α (i.e., $|\cos \theta_\alpha| = 1.0$) increases in the region of the flame where the chemical reaction effects are strong. The PDFs of $|\cos \theta_\alpha|$ and $|\cos \theta_\gamma|$, for the cases A–E, are shown elsewhere [26] and, thus, are not repeated here, but their behaviours are in agreement with the aforementioned findings by Chakraborty and Swaminathan [27].

In cases A–C, where $\sigma Da \gg 1$, ∇c predominantly aligns with the eigenvector associated with e_α (i.e., $|\cos \theta_\alpha| = 1.0$), and the strengthening of this alignment leads to an increase of $\langle |a_N||c \rangle$ from the unburned gas side until it reaches a peak value close to $c = 0.7$ before decreasing towards the burned gas side, where the effect of thermal expansion weakens. In cases D and E, where σDa remains of the order of 1.0, ∇c predominantly aligns with the eigenvector associated with e_γ (i.e., $|\cos \theta_\gamma| = 1.0$) on the unburned gas and burned gas sides of the flame, but the extent of ∇c alignment with the eigenvector associated with e_α (e_γ) increases (decreases) in the regions of high chemical reactivity.

Therefore, $\langle |a_N||c \rangle \times \delta_z/S_L$ decreases from the unburned gas side of the flame front in cases D and E where the strain rate induced by thermal expansion is of comparable strength of turbulent straining, and thus, $\langle |a_N||c \rangle \times \delta_z/S_L$ fluctuates around of value of unity for the major part of the flame front (see Figure 5). It can further be seen from Figure 6 that $\langle |a_N||c \rangle \times \tau_K$ is of order unity, fluctuating in cases D and E around 0.29, which is consistent with previous findings by Yeung et al. [31], who reported $\langle |a_N||c \rangle = 0.29/\tau_K$ for passive scalar mixing.

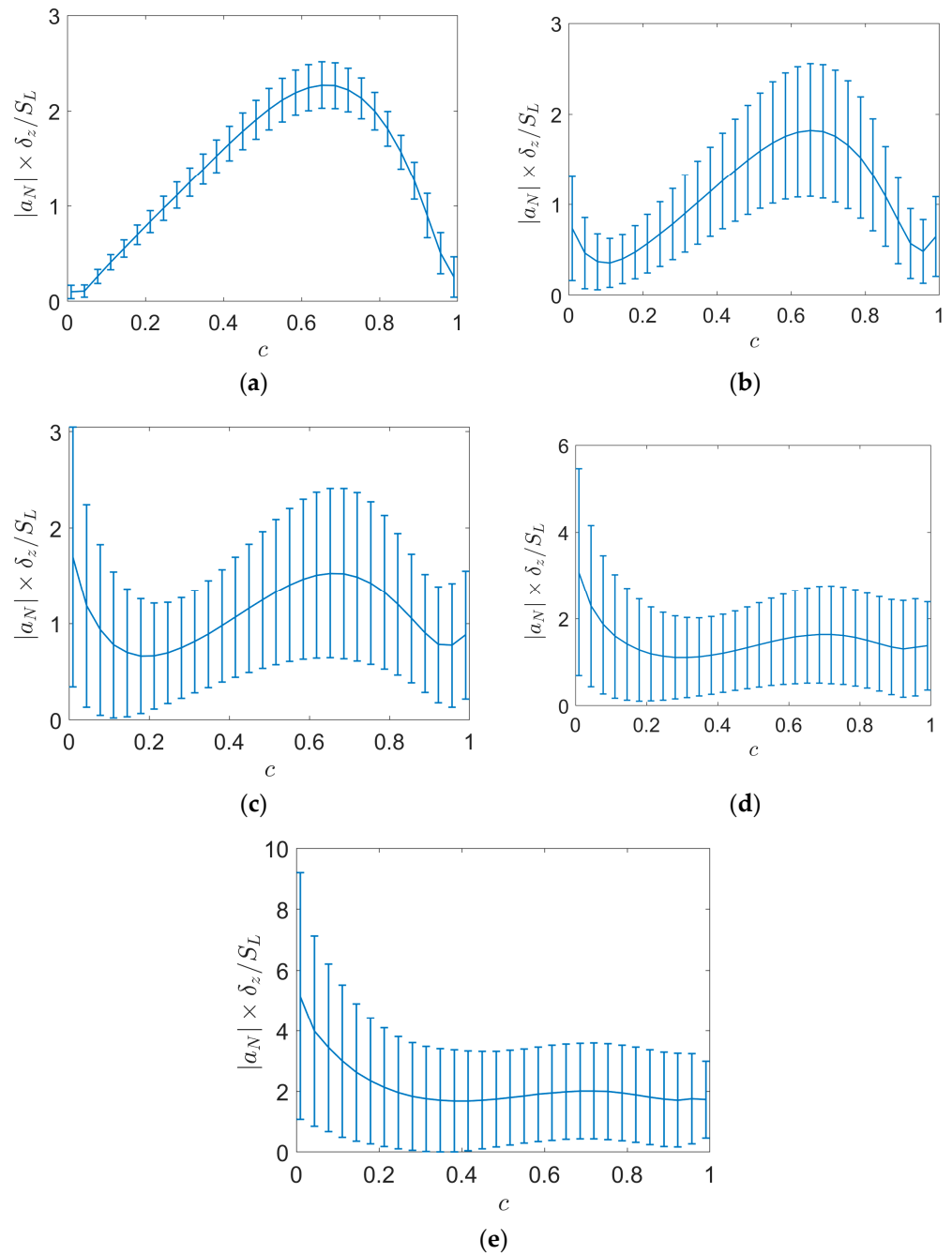


Figure 5. Variations of $\langle |a_N| |c \rangle \times \delta_z / S_L$ with c for (a–e) cases A–E.

It is worth noting that Karlovitz number scales as $Ka \sim (\delta_z / S_L) / \tau_K$, which suggests $\langle |a_N| |c \rangle \times \tau_K \sim \langle |a_N| |c \rangle \times \delta_z / S_L \times Ka^{-1}$. For Karlovitz numbers of order unity (cases A and B and probably C), the scaling of $\langle |a_N| |c \rangle$ is somewhat ambiguous (scaling with δ_z / S_L and with τ_K are equivalent). Moreover, $\langle |a_N| |c \rangle$, in cases D and E, can be scaled with respect to both δ_z / S_L and τ_K , and thus, a greater range of Ka values is needed for conclusive evidence.

The variations of $\langle T_1 |c \rangle \times \delta_z / S_L$ and $\langle T_1 |c \rangle \times \tau_K$, with c across the flame front for all cases considered here, are shown in Figures 7 and 8, respectively. The corresponding standard deviations conditional upon c are also shown in Figures 7 and 8, respectively. It can be seen from Figure 7 that $\langle T_1 |c \rangle \times \delta_z / S_L$ remains of the order of 1.0 for $c < 0.4$ but assumes values of the order of 10 in the reaction zone and of the order of 100 towards the burned gas side. Thus, perhaps $\langle T_1 |c \rangle$ cannot be scaled with the chemical timescale δ_z / S_L (see Figure 7). Figure 8 shows that $\langle T_1 |c \rangle \times \tau_K$ is of the order of 1.0 for a major part of

the flame front and of the order of 10 towards the burned gas side. Thus, the molecular diffusion rate contribution $\langle |T_1||c \rangle$ can perhaps be scaled with τ_K .

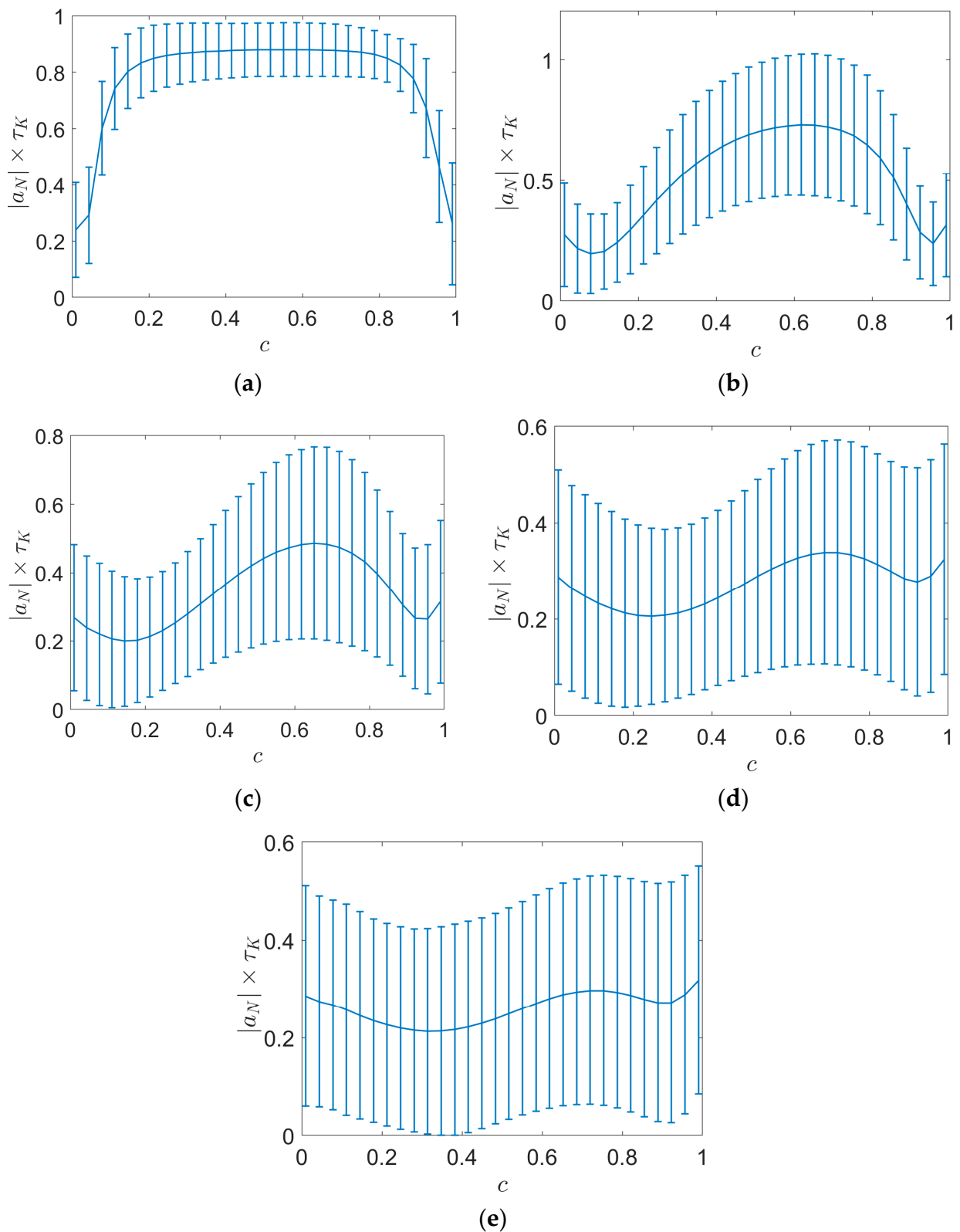


Figure 6. Variations of $\langle |a_N||c \rangle \times \tau_K$ with c for (a–e) cases A–E.

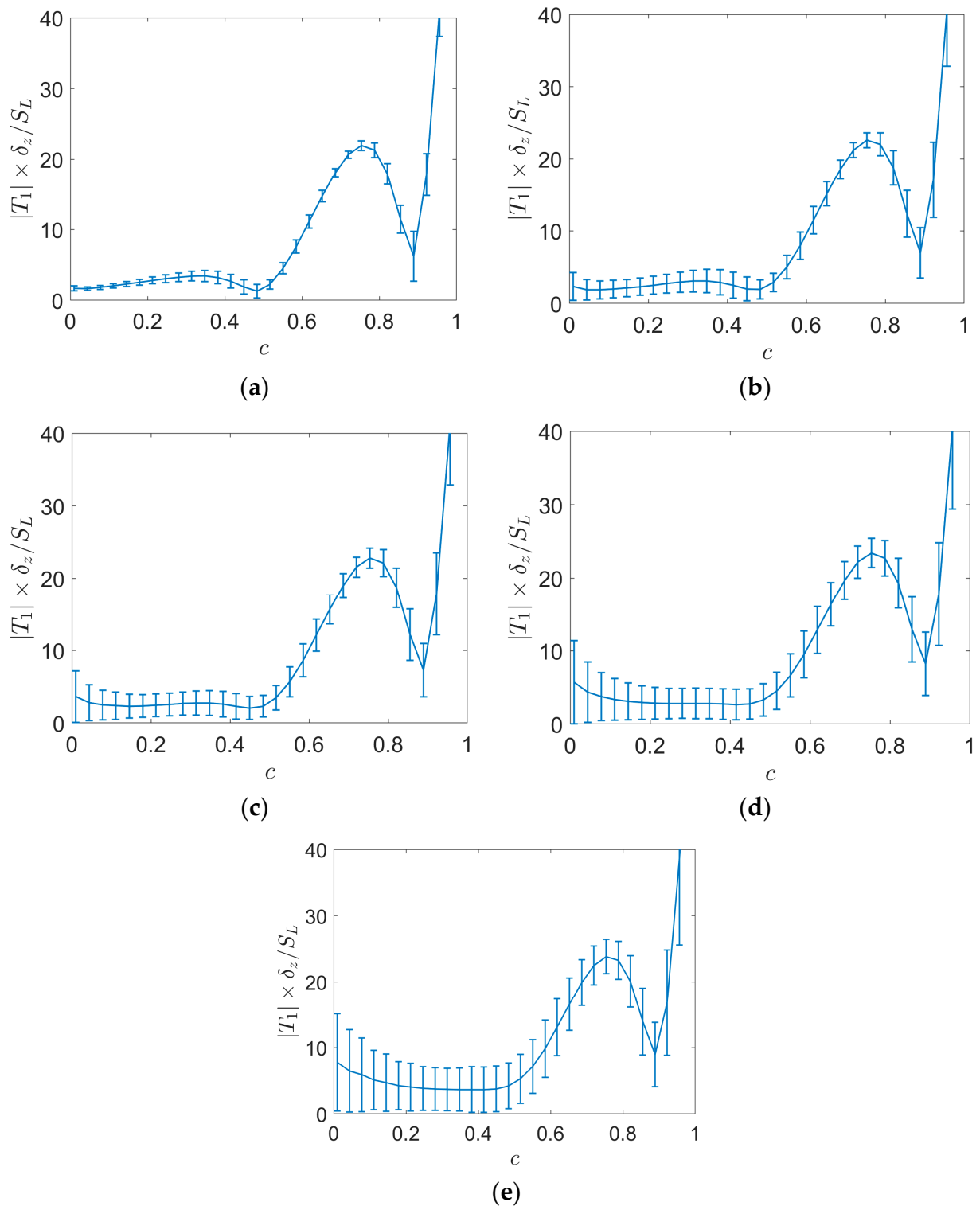


Figure 7. Variations of $\langle |T_1| |c \rangle \times \delta_z / S_L$ with c for (a–e) cases A–E.

The variations of $\langle T_2 |c \rangle \times \delta_z / S_L$ and $\langle T_2 |c \rangle \times \tau_K$ with c across the flame front for all cases considered here are shown in Figures 9 and 10, respectively, along with the standard deviations conditioned upon c . Figure 9 shows that $\langle |T_2| |c \rangle \times \delta_z / S_L$ remains of the order of 10 for a major part of the flame front and of the order of 100 towards the burned gas side. Therefore, $\langle |T_2| |c \rangle$ is unlikely to be scaled with the chemical timescale δ_z / S_L (see Figure 9). It can be seen from Figure 10 that $\langle |T_2| |c \rangle \times \tau_K$ is of the order of 1.0 for a major part of the

flame front and of the order of 10 towards the burned gas side. Thus, the reaction rate contribution $\langle |T_2||c \rangle$ can perhaps be scaled with τ_K .

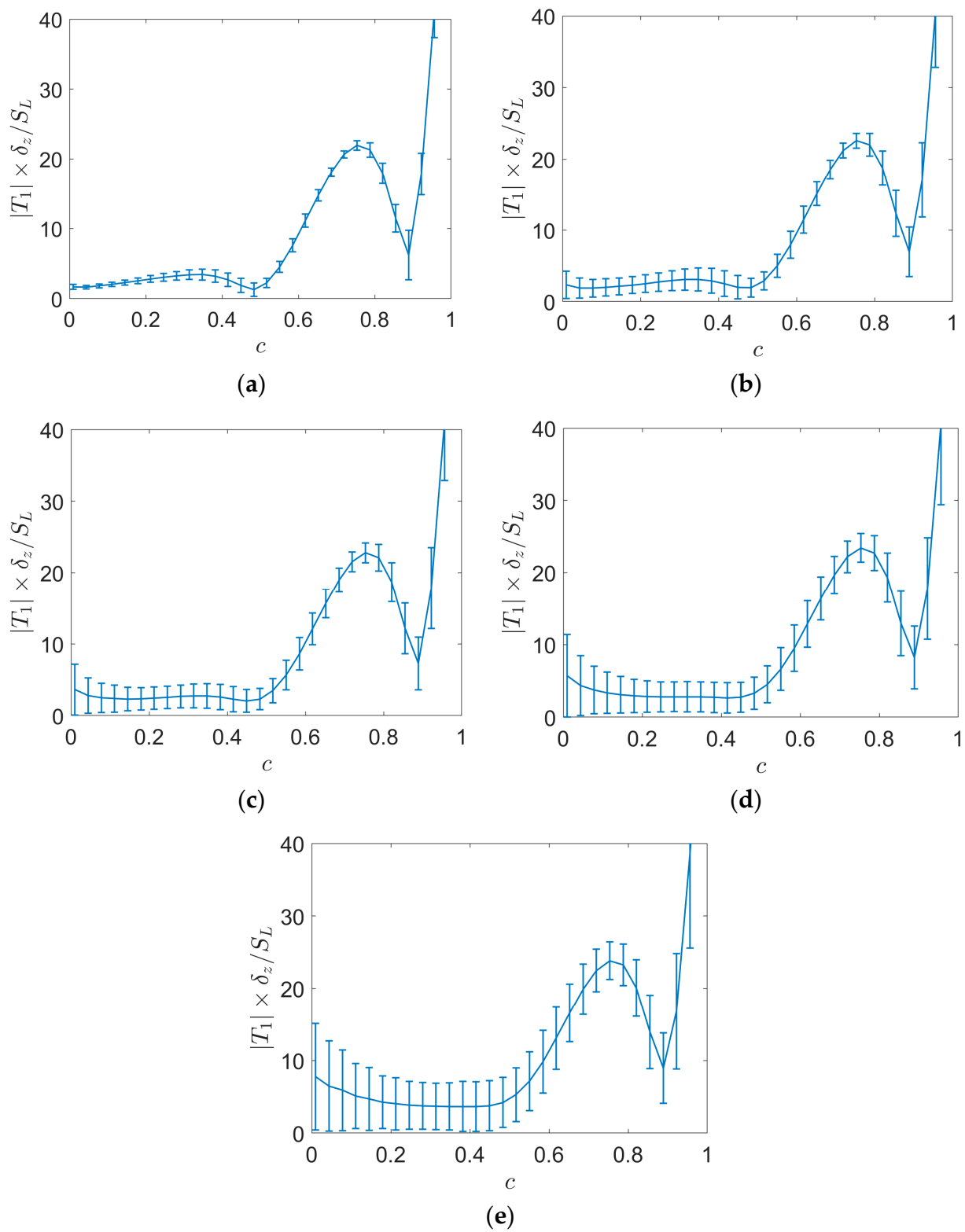


Figure 8. Variations of $\langle |T_1||c \rangle \times \tau_K$ with c for (a–e) cases A–E.

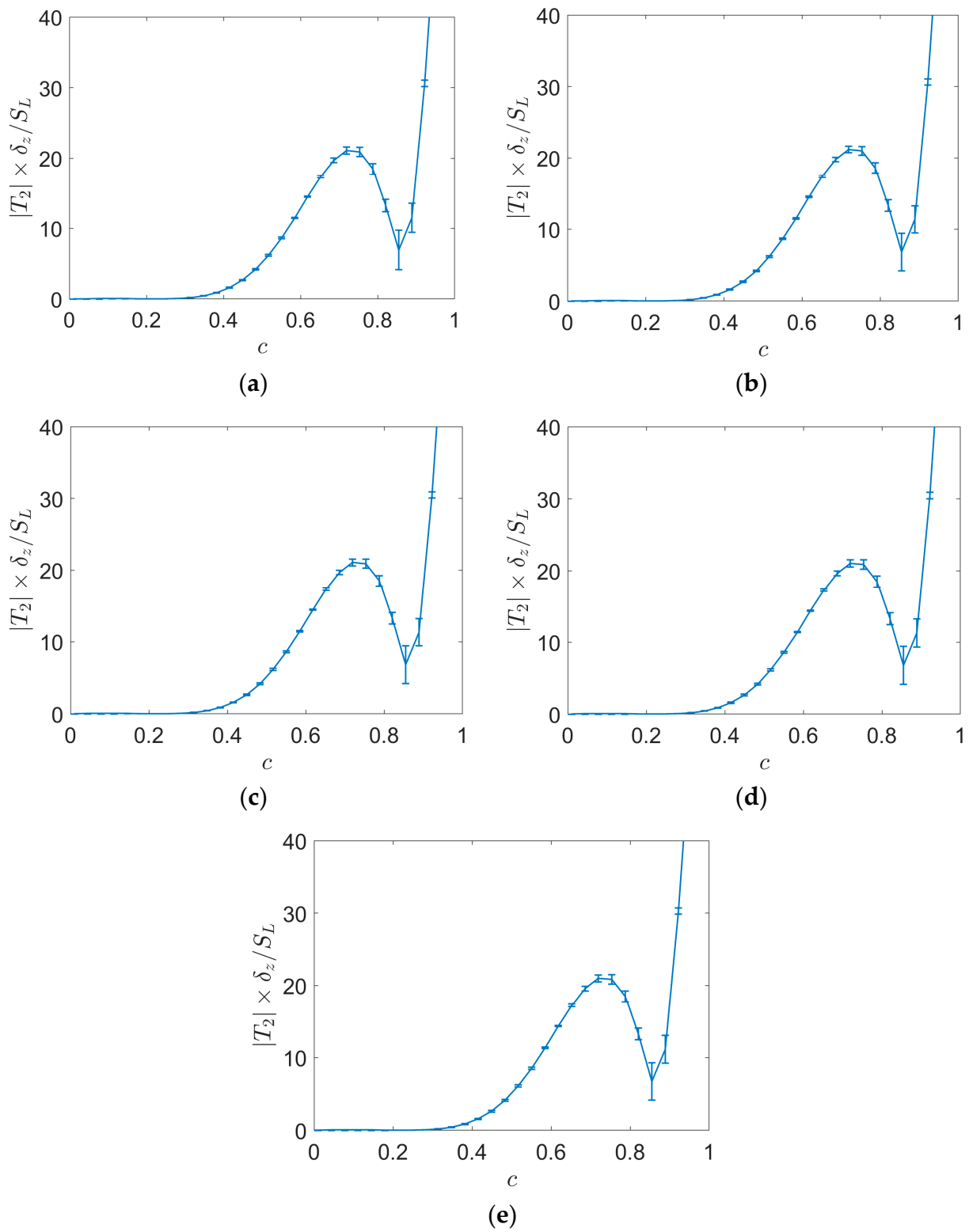


Figure 9. Variations of $\langle |T_2| |c \rangle \times \delta_z / S_L$ with c for (a–e) cases A–E.

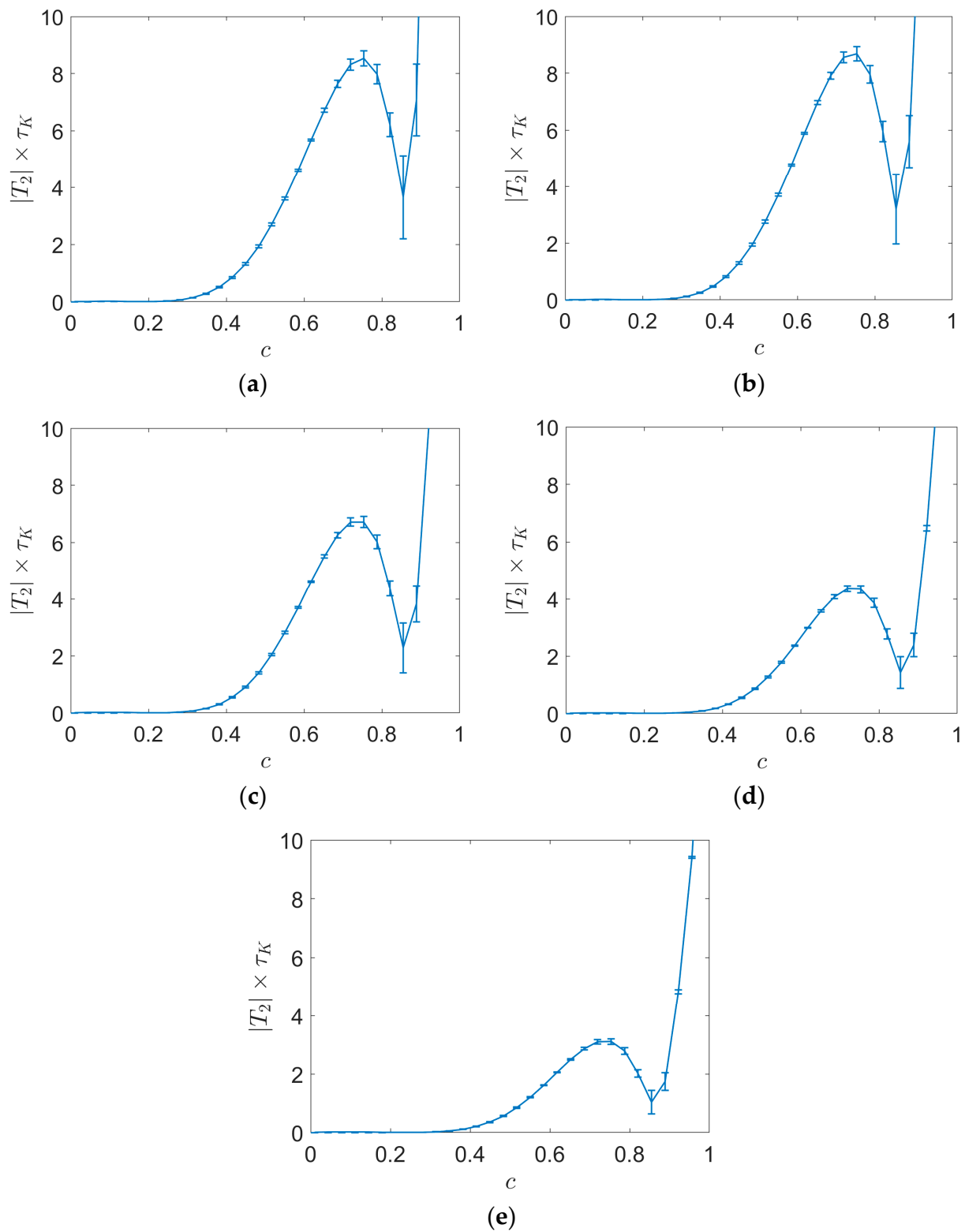


Figure 10. Variations of $\langle |T_2| |c \rangle \times \tau_K$ with c for (a–e) cases A–E.

4.4. Relative Magnitudes of Timescales τ_{flow} , τ_{md} and τ_{ch}

In order to compare the timescales associated with $|a_N|$, $|T_1|$ and $|T_2|$, the variations of the ratios $R_1 = \langle |T_1 + T_2| / |a_N| |c \rangle$, $R_2 = \langle |T_1| / |a_N| |c \rangle$ and $R_3 = \langle |T_2| / |a_N| |c \rangle$ with c for cases A–E are shown in Figure 11a–e, respectively.

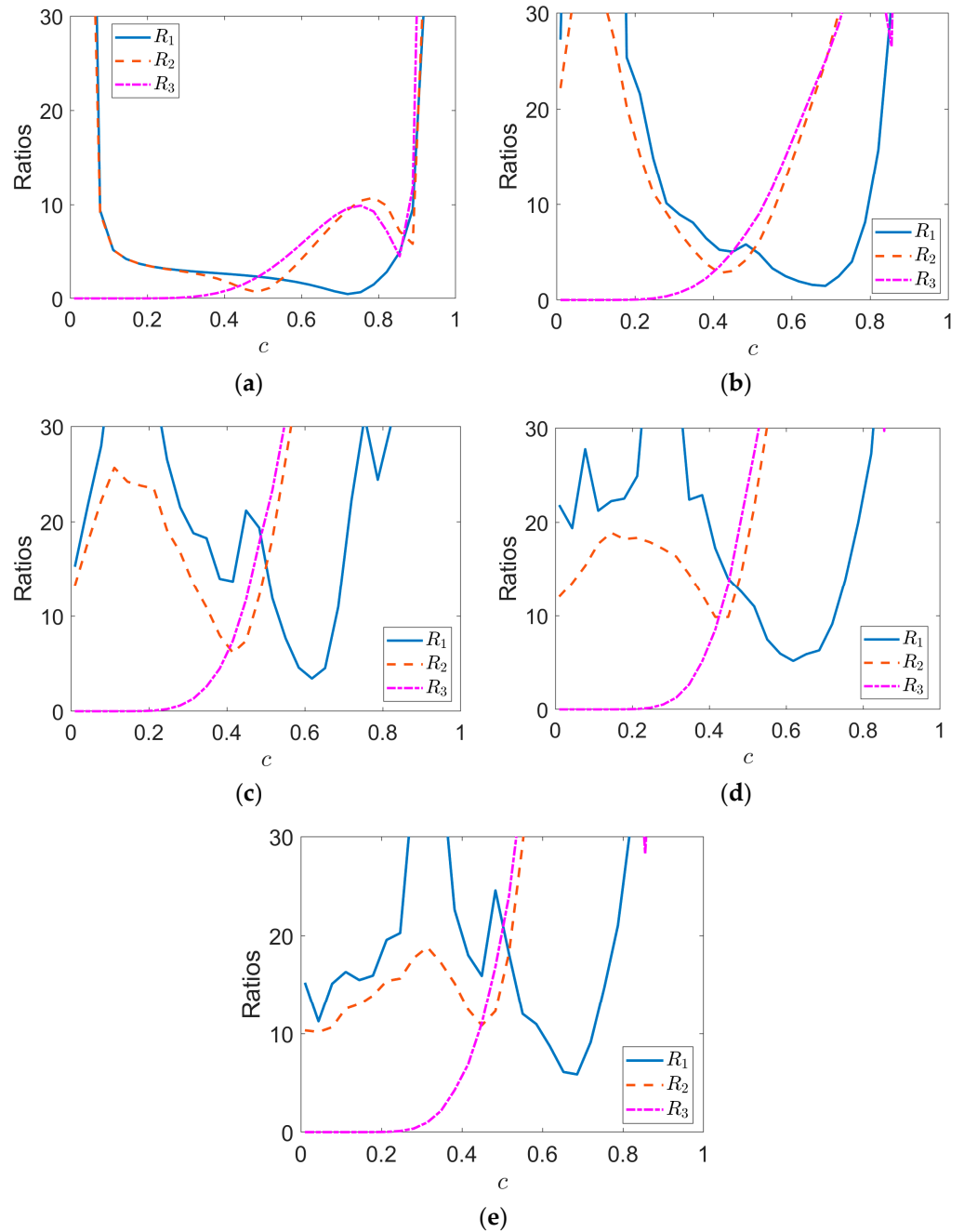


Figure 11. Variations of the ratios $R_1 = \langle |T_1 + T_2|/|a_N|c \rangle$, $R_2 = \langle |T_1|/|a_N|c \rangle$ and $R_3 = \langle |T_2|/|a_N|c \rangle$ with c for (a–e) cases A–E.

It can be seen from Figure 11 that all the ratios assume large values on both ends of the flame front because, locally, $|T_1|$ and $|T_2|$ can assume large values on both unburned and burned gas sides of the flame front because of vanishingly small values of $|\nabla c|$ in these regions (see Equations (7) and (8)). Figure 11a–e suggest that $R_2 = \langle |T_1|/|a_N|c \rangle$ and $R_3 = \langle |T_2|/|a_N|c \rangle$ assume comparable values for $c > 0.4$, which is indicative of the fact that the timescales associated with $|T_1|$ and $|T_2|$ are found to be comparable. This is indicative of the reaction–diffusion zone, which exists for all cases considered here. Moreover, a comparison between R_1 , R_2 and R_3 reveals that $|T_1|$ predominantly determines the behaviour of $|T_1 + T_2|$ towards the unburned gas side (i.e., $c < 0.4$), where $|T_2|$ assumes negligible values. Moreover, R_2 assumes a value of the order of unity in the region given by $0.2 < c < 0.4$ in cases A–C, which suggests the existence of a convective–diffusive zone in these cases. However, R_2 does not assume a value of the order of magnitude of unity in

cases D and E, which suggests that the timescale for turbulent straining becomes greater than the molecular diffusion timescale in the preheat zone for flames with high Karlovitz numbers. For $0.4 < c < 0.5$, the interaction of the flame normal gradient of the reaction rate, quantified by T_2 , with turbulence and molecular diffusion effects are found to be strong, given that $\tau_K \sim \tau_{md} \sim \tau_{ch}$. For $c \geq 0.5$, the turbulence weakly interacts with the flame normal gradients of reaction and the molecular diffusion rates in this case. Thus, turbulence does not significantly modify the reaction and hot product zones of the flame for the parameter range considered here.

5. Conclusions

The statistical behaviours of the terms originating from flame normal straining, molecular diffusion rate and chemical reaction rate in the transport equation of $|\nabla c|$ were analysed using a DNS database of statistically planar premixed turbulent flames with a range of different Karlovitz numbers. It was found that the balance between T_1 and T_2 is obtained in the reaction zone and the burned gas side (i.e., $c > 0.5$), but the reaction rate contribution T_2 is negligible for $c < 0.4$, where $(-a_N)$ and T_1 exhibit non-zero contributions. The mean values of molecular diffusion rate and reaction rate contributions conditional upon c normalised by the chemical timescale remain of the order of 10 for a major part of the flame front, whereas these terms, normalised by the Kolmogorov timescale, remain of the order of unity. The magnitude of the normal strain rate scale with both the chemical timescale and the Kolmogorov timescale for the cases considered here. A larger separation between chemical and Kolmogorov timescales (i.e., a greater range of Karlovitz numbers) is needed for conclusive evidence regarding the timescale associated with flame normal straining, but the current findings seem to suggest that the timescale associated with the molecular diffusion rate and reaction rate contributions in the transport equation of $|\nabla c|$ might be scaled with the Kolmogorov timescale. The interaction of flame normal straining with the flame normal gradient of molecular diffusion rate determines the transport of the reactive scalar gradient in the preheat zone of the flame where the timescales for turbulent straining and molecular diffusion are comparable for small values of Karlovitz numbers, but the molecular diffusion timescale turns out to be smaller than the turbulent straining timescale for high values of Karlovitz numbers. For $0.4 < c < 0.5$, the interaction of the flame normal gradient of the reaction rate, with turbulence and molecular diffusion rate effects, are found to be strong given that the timescales for the chemical reaction rate and molecular diffusion rate gradients scale with the Kolmogorov timescale. The turbulent fluid motion weakly interacts with the flame normal gradients of reaction and the molecular diffusion rates for $c \geq 0.5$, and the reaction and hot product zones of the flame remain mostly unaffected by turbulence for the cases considered here.

Although several previous analyses [4,5,24] demonstrated both qualitative and quantitative similarities between $|\nabla c|$ statistics obtained from simple and detailed chemistry DNS results, the current findings need to be confirmed based on DNS data with detailed chemistry and transport with a larger separation of Karlovitz numbers. This forms the platform for further analysis in the future. Moreover, the statistics of the suitably averaged quantities related to $|\nabla c|$ transport and its transients need to be analysed in the future for deeper understanding.

Author Contributions: Conceptualization, N.C. and C.D.; methodology, N.C.; software, N.C.; formal analysis, N.C. and C.D.; investigation, N.C. and C.D.; resources, N.C.; data curation, N.C.; writing—original draft preparation, N.C.; writing—review and editing, N.C. and C.D.; visualization, N.C. and C.D.; funding acquisition, N.C. All authors have read and agreed to the published version of the manuscript.

Funding: N.C. acknowledges the Engineering and Physical Sciences Research Council (EP/R029369/1) for the financial and computational support.

Institutional Review Board Statement: Not applicable.

Informed Consent Statement: Not applicable.

Data Availability Statement: The data that support the findings of this study are available from the corresponding author upon reasonable request.

Conflicts of Interest: The authors declare no conflicts of interest.

References

1. Vervisch, L.; Bidaux, E.; Bray, K.N.C.; Kollmann, W. Surface density function in premixed turbulent combustion modelling, similarities between probability density function and flame surface approaches. *Phys. Fluids A* **1995**, *7*, 2496–2503. [[CrossRef](#)]
2. Veynante, D.; Vervisch, L. Turbulent combustion modelling. *Prog. Energy Combust. Sci.* **2002**, *28*, 193–266. [[CrossRef](#)]
3. Kollmann, W.; Chen, J.H. Pocket formation and the flame surface density equation. *Proc. Combust. Inst.* **1998**, *27*, 927–934. [[CrossRef](#)]
4. Chakraborty, N.; Cant, R.S. Effects of strain rate and curvature on Surface Density Function transport in turbulent premixed flames in the thin reaction zones regime. *Phys. Fluids* **2005**, *17*, 65108. [[CrossRef](#)]
5. Chakraborty, N.; Hawkes, E.R.; Chen, J.H.; Cant, R.S. Effects of strain rate and curvature on Surface Density Function transport in turbulent premixed CH₄-air and H₂-air flames: A comparative study. *Combust. Flame* **2008**, *154*, 259–280. [[CrossRef](#)]
6. Sankaran, R.; Hawkes, E.R.; Chen, J.H.; Lu, T.; Law, C.K. Structure of a spatially developing turbulent lean methane–air Bunsen flame. *Proc. Combust. Inst.* **2007**, *31*, 1291–1298. [[CrossRef](#)]
7. Dopazo, C.; Cifuentes, L.; Martin, J.; Jimenez, C. Strain rates normal to approaching isoscalar surfaces in a turbulent premixed flame. *Combust. Flame* **2015**, *162*, 1729–1736. [[CrossRef](#)]
8. Wang, H.; Hawkes, E.R.; Chen, J.H.; Zhou, B.; Li, Z.; Alden, M. Direct numerical simulations of a high Karlovitz number laboratory premixed jet flame—An analysis of flame stretch and flame thickening. *J. Fluid Mech.* **2017**, *815*, 511–536. [[CrossRef](#)]
9. Sandeep, A.; Proch, F.; Kempf, A.M.; Chakraborty, N. Statistics of strain rates and Surface Density Function in a flame-resolved high-fidelity simulation of a turbulent premixed bluff body burner. *Phys. Fluids* **2018**, *30*, 065101. [[CrossRef](#)]
10. Jenkins, K.W.; Cant, R.S. DNS of turbulent flame kernels. In Proceedings of the 2nd AFOSR Conference on DNS and LES, New Brunswick, NJ, USA, 7–9 June 1999; Liu, C., Sakell, L., Beutner, T., Eds.; Kluwer Academic Publishers: New York, NY, USA, 1999; pp. 192–202.
11. Cant, R.S. Direct Numerical Simulation of premixed turbulent flames. *Phil. Trans. R. Soc. Lond. A* **1990**, *357*, 3583–3604. [[CrossRef](#)]
12. Wray, A.A. *Minimal Storage Time Advancement Schemes for Spectral Methods*; Unpublished Report; NASA Ames Research Center: Mountain View, CA, USA, 1990.
13. Poinot, T.; Lele, S.K. Boundary conditions for direct simulation of compressible viscous flows. *J. Comp. Phys.* **1992**, *101*, 104–129. [[CrossRef](#)]
14. Rogallo, R.S. *Numerical Experiments in Homogeneous Turbulence*; NASA Technical Memorandum 81315; NASA Ames Research Center: Mountain View, CA, USA, 1981.
15. Batchelor, G.K.; Townsend, A.A. Decay of turbulence in final period. *Proc. R. Soc. Lond.* **1948**, *A194*, 527–543.
16. Klein, M.; Chakraborty, N.; Ketterl, S. A comparison of strategies for Direct Numerical Simulation of turbulence chemistry interaction in generic planar turbulent premixed flames. *Flow Turb. Combust.* **2017**, *199*, 955–971. [[CrossRef](#)]
17. Peters, N. *Turbulent Combustion*, 1st ed.; Cambridge University Press: Cambridge, UK, 2000.
18. Rutland, C.; Trouvé, A. Direct Simulations of premixed turbulent flames with nonunity Lewis numbers, *Combust. Flame* **1993**, *94*, 41–57. [[CrossRef](#)]
19. Trouvé, A.; Poinot, T. The evolution equation for flame surface density in turbulent premixed combustion. *J. Fluid Mech.* **1994**, *278*, 1–31. [[CrossRef](#)]
20. Boger, M.; Veynante, D.; Boughanem, H.; Trouvé, A. Direct Numerical Simulation analysis of flame surface density concept for Large Eddy Simulation of turbulent premixed combustion. *Proc. Combust. Inst.* **1998**, *27*, 917–925. [[CrossRef](#)]
21. Charlette, F.; Meneveau, C.; Veynante, D. A power law wrinkling model for LES of premixed turbulent combustion, Part I: Non dynamic formulation and initial tests. *Combust. Flame* **2002**, *131*, 159–180. [[CrossRef](#)]
22. Han, I.; Huh, K.Y. Roles of displacement speed on evolution of flame surface density for different turbulent intensities and Lewis numbers for turbulent premixed combustion. *Combust. Flame* **2008**, *152*, 194–205. [[CrossRef](#)]
23. Grout, R.W.; Swaminathan, N. Interaction of turbulence and scalar fields in premixed flames. *Phys. Fluids* **2006**, *18*, 045102.
24. Chakraborty, N.; Kolla, H.; Sankaran, R.; Hawkes, E.R.; Chen, J.H.; Swaminathan, N. Determination of three-dimensional quantities related to scalar dissipation rate and its transport from two-dimensional measurements: Direct Numerical Simulation based validation. *Proc. Combust. Inst.* **2013**, *34*, 1151–1162. [[CrossRef](#)]
25. Keil, F.B.; Amzehnhoff, M.; Ahmed, U.; Chakraborty, N.; Klein, M. Comparison of flame propagation statistics extracted from DNS based on simple and detailed chemistry Part 1: Fundamental flame turbulence interaction. *Energies* **2021**, *14*, 5548. [[CrossRef](#)]
26. Ahmed, U.; Chakraborty, N.; Klein, M. Insights into the bending effect in premixed turbulent combustion using the Flame Surface Density transport. *Combust. Sci. Technol.* **2019**, *191*, 898–920. [[CrossRef](#)]
27. Chakraborty, N.; Swaminathan, N. Influence of Damköhler number on turbulence-scalar interaction in premixed flames, Part I: Physical Insight. *Phys. Fluids* **2017**, *19*, 045103. [[CrossRef](#)]
28. Batchelor, G.K. The effect of homogeneous turbulence on material lines and surfaces. *Proc. R. Soc. Lond. A* **1952**, *231*, 349–366.

29. Batchelor, G.K. Small-scale variation of convected quantities like temperature in turbulent fluid Part 1. General discussion and the case of small conductivity. *J. Fluid Mech.* **1959**, *5*, 113–133. [[CrossRef](#)]
30. Gibson, C. Fine structure of scalar fields mixed by turbulence. I: Zero gradient points and minimal gradient points. *Phys. Fluids* **1968**, *11*, 2305–2315. [[CrossRef](#)]
31. Yeung, P.K.; Girimaji, S.S.; Pope, S.B. Straining and scalar dissipation on material surfaces in turbulence: Implication for flamelets. *Combust. Flame* **1990**, *79*, 340–365. [[CrossRef](#)]

Disclaimer/Publisher’s Note: The statements, opinions and data contained in all publications are solely those of the individual author(s) and contributor(s) and not of MDPI and/or the editor(s). MDPI and/or the editor(s) disclaim responsibility for any injury to people or property resulting from any ideas, methods, instructions or products referred to in the content.